

Core polarizability of rubidium using spectroscopy of the ng to nh, ni Rydberg transitions

S.J. Berl, C.A. Sackett,* and T.F. Gallagher

Department of Physics, University of Virginia, Charlottesville, Virginia 22904, USA

J. Nunkaew

*Thailand Center of Excellence in Physics, Ministry of Higher Education, Science,
Research and Innovation, 328 Si Ayutthaya Road, Bangkok, 10400, Thailand*

(Dated: September 30, 2020)

We present a precise measurement of the rubidium ionic core polarizability. The results can be useful for interpreting experiments such as parity violation or black-body radiation shifts in atomic clocks since the ionic core electrons contribute significantly to the total electrical polarizability of rubidium. We report a dipole polarizability $\alpha_d = 9.116 \pm 0.009 a_0^3$ and quadrupole polarizability $\alpha_q = 38.4 \pm 0.6 a_0^5$ derived from microwave and radio-frequency spectroscopy measurements of Rydberg states with large angular momentum. By using a relatively low principal quantum number ($17 \leq n \leq 19$) and high angular momentum ($4 \leq \ell \leq 6$), systematic effects are reduced compared to previous experiments. We develop an empirical approach to account for non-adiabatic corrections to the polarizability model. The corrections have less than a 1% effect on α_d but almost double α_q from its adiabatic value, bringing it into much better agreement with theoretical values.

I. INTRODUCTION

The electric polarizability of an atom is of significant interest and importance. Accurate polarizability values are needed for many experiments, including atomic clocks, quantum computation, parity-nonconservation, thermometry, and studies of long-range molecules [1–5]. Polarizability measurements are also useful as benchmarks for theoretical calculations since the polarizability depends on the dipole matrix elements of the atomic wave functions, which are difficult to obtain using conventional spectroscopy. Calculation of matrix elements from first principles is very challenging for multi-electron atoms, so comparisons to experimental quantities, like polarizabilities, provide important checks. These motivations have prompted a series of improving polarizability measurements over the past several decades [6–13]. One promising new approach is tune-out spectroscopy [14], where the ac electric polarizability of an atom vanishes and the wavelength at which that occurs is measured. This technique can provide orders of magnitude improvement in the accuracy of the dipole matrix elements [10, 11, 13, 15].

Theoretical interpretation of the polarizability is simplest for alkali atoms, where most of the effect comes from the single valence electron. However, the contribution of the core electrons cannot be ignored. For instance, the core contributes about 3% to the total polarizability of a Rb atom [3], which is large compared to the 0.2% accuracy of a measurement such as in Ref. [9]. It can be useful to evaluate and subtract the core contribution from a measurement to obtain the valence polarizability alone, since this provides the most direct connection to the matrix elements of the valence wave functions. This

approach has been used with both dc and tune-out measurements [10], but it is limited by the accuracy to which the core polarizability is known. We present here a new experimental measurement of the core polarizability of Rb, with an accuracy approximately a factor of four better than previously achieved. We expect this to be useful as tune-out spectroscopy and other polarizability measurement techniques continue to improve.

The core polarizability is obtained in our experiment through microwave spectroscopy of atomic Rydberg states of high orbital angular momentum ℓ . When the valence electron is far from the core, the atom behaves much like hydrogen; however in any atom other than hydrogen, the Rydberg electron can both penetrate and polarize the ion core, depressing the atomic energy below the analogous hydrogenic energy. Due to the ℓ dependent centrifugal barrier keeping the Rydberg electron away from the ion core, Rydberg states of high ℓ ($\ell \geq 4$ for Rb) have negligible core penetration. However, core polarization remains, and by comparing the energies of the high ℓ states to the corresponding hydrogenic energies, the core polarizability can be determined [16, 17]. This method was previously used in Rb with Rydberg states having principal quantum number n in the range of 27 to 30 [12]. The accuracy of the spectroscopy measurements was principally limited by Stark shifts from stray dc electric fields. The dc polarizability of a Rydberg atom as a whole is very large, so even fields of 100 mV/cm can be significant [12]. To address this problem, the work here uses lower principal quantum numbers: $n = 17$ to 19. Since the atomic polarizability scales as n^7 , this reduces the electric field sensitivity by a factor of about twenty-five compared to previous work from our group [12]. Our analysis combines our new results, previous measurements from [12], and recent measurements by Moore *et al.* in the range $n = 38$ to 43 [18].

Because the valence electron produces a non-uniform

* sackett@virginia.edu

field at the ion core, the polarization energy of the Rydberg atom depends on both the dipole polarizability α_d and the quadrupole polarizability α_q of the core [16, 17]. Explicitly, the polarization energy is given, in atomic units, by [17, 19]

$$W = -\frac{1}{2}\alpha_d \left\langle \frac{1}{r^4} \right\rangle_{n\ell} - \frac{1}{2}\alpha_q \left\langle \frac{1}{r^6} \right\rangle_{n\ell}, \quad (1)$$

where r is the distance from the valence electron to the nucleus, and $\langle \frac{1}{r^4} \rangle_{n\ell}$ and $\langle \frac{1}{r^6} \rangle_{n\ell}$ are the expectation values of the squares of the expectation values of the field and field gradient at the ion core due to the static probability distribution of the $n\ell$ electron. Because of the centrifugal barrier, $\langle \frac{1}{r^4} \rangle$ and $\langle \frac{1}{r^6} \rangle$ are highly dependent on ℓ , and measuring the separation between high ℓ states of the same n allows us to determine α_d and α_q .

Eq. (1) is often termed the adiabatic core polarization model since it is based on the assumption that the Rydberg electron cloud is static. Of course, the Rydberg electron is not static, and Whitelaw and van Vleck pointed out that Eq. (1) is a limiting case of a shift arising from second order perturbation theory [20]. In particular, Eq. (1) is valid when the excited states of the ion lie far above the its ground state compared to the energy spread of the Rydberg states involved. Detailed derivations of Eq. (1) from the perturbation theory expressions were subsequently given by Mayer and Mayer and van Vleck and Whitelaw [21, 22]. Although the adiabatic approximation of Eq. (1) is reasonably good for Rb, it is not adequate for our purposes. Here we develop an empirical method to account for the nonadiabatic effects. Specifically, we compare Eq. (1) to the expression of van Vleck and Whitelaw using several simplifications [22]. This comparison results in correction factors k_d and k_q which must be applied to Eq. (1), both of which are unity in the adiabatic approximation. Our estimates of k_d and k_q differ from unity by less than 10%, and their introduction alters α_d by less than 1%, but almost doubles α_q from its adiabatic value and brings it into much better agreement with theoretical values [3, 12, 23, 24].

In the sections that follow, we describe the principle and setup of the experiments, the spectroscopic results, the development of the non-adiabatic corrections, the analysis of the polarizabilities, and finally our conclusions.

II. EXPERIMENTAL APPROACH

In order to interpret the energy shifts of the Rydberg state in terms of the core polarizability, it is necessary for the valence electron to remain far from the core at all times. In addition to large n , this also requires the use of large angular momentum quantum number ℓ . Core penetration in a Rydberg state causes its fine structure splitting to differ significantly from that of hydrogen. Such distortions are observed in Rb for $\ell \leq 3$, so we use only states with $\ell \geq 4$. The atoms are excited using

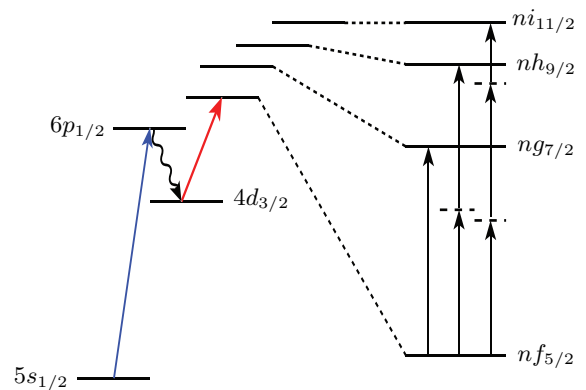


FIG. 1. Atomic states used in this measurement. Rubidium atoms in the $5s_{1/2}$ ground state are optically excited to $6p_{1/2}$, allowed to spontaneously decay to $4d_{3/2}$, and are then optically driven to the $nf_{5/2}$ Rydberg state for $n = 17 - 19$. The expanded diagram on the right shows microwave transitions from nf to ng , nh , and ni states using one, two, and three photon excitations, respectively. The $f - g$ interval is about 15 GHz, the $g - h$ interval is about 3 GHz, and the $h - i$ interval is about 1 GHz; the precise values depend on n .

the scheme shown in Fig. 1 where a laser pulse first excites the atoms from the $5s_{1/2}$ ground state to the $6p_{1/2}$ excited state. About a third of the excited atoms spontaneously decay to the long-lived $4d_{3/2}$ state, from which they are excited by a second laser pulse to the $nf_{5/2}$ Rydberg state. From there, microwave and radio frequency pulses drive transitions to the ng , nh and ni states. We use the $g - h$ and $h - i$ intervals to determine the dipole (α_d) and quadrupole (α_q) polarizabilities of Rb^+ .

The experiment is performed in an atomic beam apparatus, shown in Fig. 2. The Rydberg atoms are produced between two electric field plates separated by 1.8 cm. A potential difference of up to 7 kV can be applied between the plates. After the microwave pulse is applied, the electric field is ramped to a value sufficient to ionize the Rydberg states. By carefully controlling the timing and amplitude of the ramp, the atom ionization process can be made state selective such that atoms in $\ell \geq 4$ states are ionized while the nf atoms remain neutral. Any ions produced are detected using a microchannel plate operating in analog mode with spatially integrated channels. The resulting signal current is accumulated using a gated integrator to produce the spectroscopy signal.

The laser excitation pulses are produced by a pair of home-built dye lasers. The first pulse is at a wavelength of 421.5 nm, and is produced using Stilbene 420 dye pumped by the third harmonic of a Quanta-Ray Nd:YAG laser. The second pulse is tuned between 712 nm and 720 nm to populate the desired nf state. This laser uses LD720 dye, pumped by the second harmonic of a Continuum Nd:YAG laser. Both laser pulses have a 20 ns duration, and the second pulse is delayed by 250 ns with respect to the first. Both lasers are linearly polarized perpendicular to the electric field plates. While the $6p$ fine

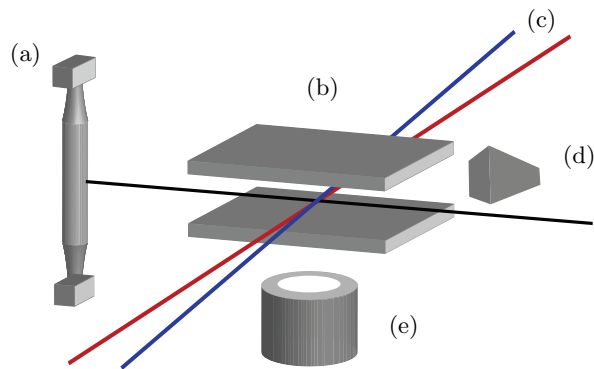


FIG. 2. Experimental apparatus (not to scale). A rubidium atomic beam is emitted from an oven (a) and passes between electric field plates (b), which are separated by 1.8 cm. Two pulsed laser beams (c) excite the atoms into Rydberg states, and microwaves from the horn (d) drive Rydberg state transitions. An electric field is applied to ionize the Rydberg atoms, and the ions are detected with microchannel plate (e).

structure is resolved by laser tuning, the nf fine structure is not.

The lifetimes of the $17f$, $18f$, and $19f$ states are 3.2, 3.8, and $4.5 \mu\text{s}$, respectively [19], and the microwave spectroscopy pulses are applied $1 \mu\text{s}$ after the second laser pulse. In the case of the nf to ng transition, a single-photon transition is driven with a microwave frequency ranging from 11 to 17 GHz, depending on n . For the nf to nh transition, a two-photon transition is driven with microwaves at half the transition frequency, between 7 and 10 GHz. For the three-photon nf to ni transition, the two-photon microwave frequency is detuned from the nh state, and we apply a rf frequency near 1 GHz to couple nh to ni . These three excitation schemes are illustrated in Fig. 1. The microwaves are produced by an Agilent 83622B frequency synthesizer coupled to one of two microwave horns. The rf field is produced by coupling a HP 8673C synthesizer to one of the electric field plates. In all cases, the duration of the spectroscopy pulse is $1 \mu\text{s}$.

For each measurement, the microwave frequency is swept across the resonance. The measurement results of each frequency step in the sweep are averaged over ten experimental cycles, and the sweep in its entirety is repeated five times. The resulting signals are averaged to produce a line profile, such as the example data shown in Fig. 3. The profiles are least-squares fit to Lorentzian functions to determine the line centers. Uncertainty in the line center is taken from the uncertainty estimate of the fit. However, in cases where the line center uncertainty from the fit is below 10% of the fit linewidth, we instead assigned an uncertainty of 10% of the linewidth to reflect the fact that the actual lineshape is not well characterized.

Several sources of systematic uncertainty must be taken into account, including dc Stark shifts, ac Stark shifts, Zeeman shifts, and fine structure splitting.

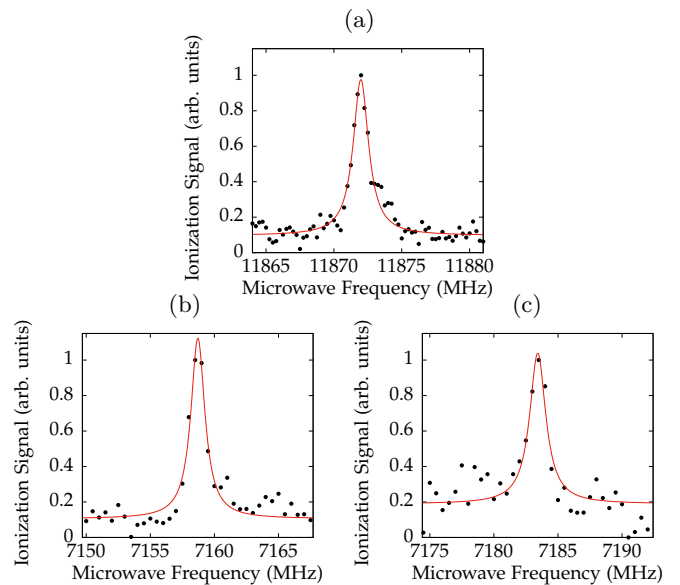


FIG. 3. Example spectroscopy line profiles. (a) Single-photon $19f_{5/2} - 19g_{7/2}$. (b) Two-photon $19f_{5/2} - 19h_{9/2}$. (c) Three-photon $19f_{5/2} - 19i_{11/2}$ with an applied rf frequency of 720 MHz.

Although dc Stark shifts are reduced by operating at relatively low n , they must still be accounted for. The conducting field plates suppress electric fields parallel to the plates, but any residual voltage difference produces a significant field normal to the plates. We are able to apply a bias voltage across the plates during the experiment, and Fig. 4(a) shows how the $nf - ng$ transition frequency varies as a function of the resulting bias field. We fit such data to a parabola and then set the bias voltage to the vertex of the fit. We perform this calibration daily, and observe day-to-day variations of about 0.15 V/cm, corresponding to Stark shifts of the $nf - ng$ transition up to approximately 0.6 MHz. The apparatus provides no direct way to measure or control the transverse electric field components, but other experiments with similar geometries show that the transverse fields are typically below 0.1 V/cm [12]. We computed the expected Stark shift at this field value and found for $n = 19$ values of 0.25 MHz on the $f - g$ transition, 0.82 MHz on the $f - h$ transition, and 1.58 MHz on the $f - i$ transition. These values are in good agreement with the measured field sensitivity. These shifts are the dominant systematic uncertainty for the measurement. We scale each shift appropriately with n and add it in quadrature to the corresponding experimental frequency error [25].

There are no ac Stark shifts on the single-photon nf to ng transitions, but there are on the multi-photon transitions. These shifts are manifested as linear variations of the transition frequency as a function of microwave or rf power. We compensate for them by taking data over a range of powers and extrapolating the results to zero power. Example data are shown in Fig. 4(b) and (c). The ac Stark shift is largest for the three-photon $nf - ni$

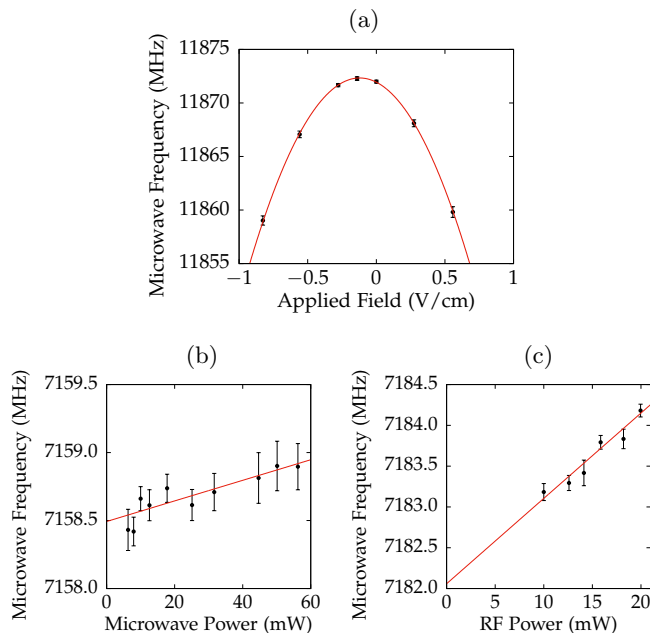


FIG. 4. a) Measurement of the dc Stark shift on the $19f_{5/2} - 19g_{7/2}$ transition. For spectroscopy, the bias voltage is set to the vertex of the curve. b) Measurement of the ac Stark shift on the two-photon $19f_{5/2} - 19h_{9/2}$ transition. The line is a linear fit showing the extrapolation to zero microwave power. c) Measurement of the ac Stark shift on the three-photon $19f_{5/2} - 19i_{11/2}$ transition. The microwave frequency is swept at a constant 50 mW power. The rf frequency is kept constant at 720 MHz and its power is varied. The line is again a linear fit.

transition, and the shift depends on the two-photon detuning from the nh state. For these measurements, the microwave and rf powers were independently varied and extrapolated to zero. For each n we used, at least two different two-photon detuning values, with at least one on each side of the h state resonance. The values obtained were consistent with the estimated uncertainties. In all cases, the extrapolation to zero power was performed using an error-weighted least squares fit to the data, and the uncertainty from this fit is reported as the uncertainty in the transition frequency measurement. The resulting values are reported in Table I. For the majority of the transitions reported here, at least two measurements were completed on different days, and the results agreed within the stated uncertainty.

The linearly polarized laser beams produce a symmetric distribution of m levels, so we expect no first-order Zeeman shift. However, the measured background field of about 0.5 G gives a Zeeman energy similar to the fine-structure splitting, so computation of the expected spectrum is complicated. Instead we applied a bias field comparable to the background field and observed shifts of about 0.1 MHz. We include this as a source of systematic uncertainty in the results.

In hydrogen, the fine structure (FS) splittings of the

$n = 17 - 19$ g , h and i states range from 1.8 MHz to 0.6 MHz. This is comparable to or less than our experimental linewidth, so the fine structure is not well resolved, but it is significant compared to our measurement accuracy. To avoid uncertainty due to unresolved FS we take advantage of the fact that the excitation scheme of Fig. 1 ensures that the Rydberg atoms are always in the lower j fine structure state, $j = \ell - 1/2$. Accordingly, we have measured the intervals given in Table I.

We expect the $\ell \geq 4$ FS splittings in Rb to be similar to those of hydrogen, because the $\ell \geq 4$ states should not penetrate the core and the core polarization effect is independent of j . To verify this, we retuned the initial laser excitation pulse to the $6p_{3/2}$ state, which then allowed excitation of both the $nf_{5/2}$ and $nf_{7/2}$ states. The $nf_{7/2} - ng_{7/2}$ transition is suppressed due to small Clebsch-Gordan coefficients, but we observed the $nf_{7/2} - ng_{9/2}$ transition. Using the known f -state FS splitting [26], we obtained a value for the $17g$ FS splitting of 1.83 ± 0.06 MHz. This is in agreement with the hydrogenic value of 1.78 MHz and supports the conclusion that the g -states are non-penetrating [27]. We therefore use the hydrogen FS values for the $\ell \geq 4$ states. For the analysis described below, we use transition frequencies from which the FS shift has been removed by referencing the transition to the center of gravity of the FS manifold. These frequencies are also listed in Table I.

III. ANALYSIS & DISCUSSION

In our analysis we assume that core penetration does not occur in Rb states of $\ell \geq 4$ and that relativistic and exchange effects are negligible. In the adiabatic core polarization model the electric field from the quasistatic charge distribution of the Rydberg $n\ell$ electron polarizes the ion core, which results in the polarization energy shift of the Rydberg $n\ell$ state relative to the hydrogenic $n\ell$ energy. The shift is given by Eq. (1), which we here rewrite as

$$W = -\frac{1}{2}\alpha_d^{(a)} \left\langle \frac{1}{r^4} \right\rangle_{n\ell} - \frac{1}{2}\alpha_q^{(a)} \left\langle \frac{1}{r^6} \right\rangle_{n\ell}, \quad (2)$$

where the superscripts denote the use of the adiabatic approximation. If we assume the $n\ell$ wavefunctions to be hydrogenic, there are closed form expressions for the required expectation values [17, 19, 28]. As a result, it is a straightforward matter to extract $\alpha_d^{(a)}$ and $\alpha_q^{(a)}$ from the high- ℓ Rydberg energies.

Equation (2) gives the energy shift of a state relative to the corresponding state of hydrogen, but we do not have accurate values for the absolute energies of the nf states, so we cannot evaluate the energies of the high- ℓ states relative to hydrogen. Instead, we consider the energy difference between two states $n\ell$ and $n\ell'$. Since the hydrogenic energies are independent of ℓ , the energy

TABLE I. Measured transition intervals and intervals referenced to the centers of gravity of the fine-structure doublets in MHz for $n = 17 - 19$, $f - g$, $f - h$, and $f - i$. The uncertainties reported correspond to statistical uncertainties added in quadrature with a possible 0.1 V/cm uncontrolled static electric field and an experimentally determined Zeeman shift.

n	$f_{5/2} - g_{7/2}$	$f_{cg} - g_{cg}$	$f_{5/2} - h_{9/2}$	$f_{cg} - h_{cg}$	$f_{5/2} - i_{11/2}$	$f_{cg} - i_{cg}$
17	16528.7(2)	16547.3(2)	19929.5(5)	19947.8(5)	20992.5(10)	21010.6(10)
18	13945.2(2)	13960.9(2)	16815.6(6)	16831.0(6)	17713.2(12)	17728.5(12)
19	11872.3(3)	11885.7(3)	14317.0(8)	14330.2(8)	15082.9(18)	15096.0(18)

difference is

$$\Delta W = -\frac{1}{2}\alpha_d^{(a)}\Delta_d^{(a)} - \frac{1}{2}\alpha_q^{(a)}\Delta_q^{(a)}, \quad (3)$$

where

$$\Delta_d^{(a)} \equiv \left\langle \frac{1}{r^4} \right\rangle_{n\ell} - \left\langle \frac{1}{r^4} \right\rangle_{n\ell'} \quad (4)$$

and

$$\Delta_q^{(a)} \equiv \left\langle \frac{1}{r^6} \right\rangle_{n\ell} - \left\langle \frac{1}{r^6} \right\rangle_{n\ell'} \quad (5)$$

The energy difference ΔW corresponds to the FS-corrected transition frequencies reported in Table I.

Figure 5 is a plot of $2\Delta W/\Delta_d^{(a)}$ vs. $\Delta_q^{(a)}/\Delta_d^{(a)}$. The solid black circles show our values for (ℓ, ℓ') pairs (4, 5) and (5, 6). We also include results from Lee *et al.* [12] as open blue circles, and from Moore *et al.* [18] as solid red squares. Lee measured the energy shifts W of individual states relative to hydrogen, so for those points the x coordinates are $\langle r^{-6} \rangle_{n\ell}/\langle r^{-4} \rangle_{n\ell}$ and the y coordinates are $2W/\langle r^{-4} \rangle_{n\ell}$. Moore measured the transition frequencies between different n levels, so the hydrogenic contributions $-R/n^2$ are subtracted in ΔW , where R is the mass-adjusted Rydberg constant for ^{85}Rb .

To obtain estimates for the adiabatic polarizabilities, we fit the data points to a line, with the results shown in Table II. The heavy line in the figure shows the best fits to all the data. The other lines illustrate the uncertainty range of the fits. The fit uncertainties are calculated differently than by Lee *et al.*: here we estimate the error in a parameter as the change required to increase χ^2/dof by one when $\chi^2/\text{dof} < 1$, or to double χ^2 when $\chi^2/\text{dof} \geq 1$. In Ref. [12], the errors were determined by increasing χ^2/dof by one in all cases. For the Lee data alone, we now obtain $\alpha_d^{(a)} = 9.12(4)$ and $\alpha_q^{(a)} = 14(4)$, with $\chi^2/\text{dof} = 4$. In comparison, Lee *et al.* reported $\alpha_d^{(a)} = 9.12(2)$ and $\alpha_q^{(a)} = 14(3)$. Note that the low value for χ^2/dof for the present data alone reflects the fact that our uncertainty is dominated by systematic error from horizontal bias fields.

It is apparent from the table and the graph that the different data sets are not entirely consistent. In particular, the $h - i$ frequencies measured here yield points that lie below the overall best-fit line. The other points

TABLE II. Calculated values of the dipole and quadrupole polarizabilities, using the adiabatic core polarization model. Data sets are Berl (present work), Lee [12], and Moore [18]. Values in parentheses are the estimated uncertainties. The goodness-of-fit parameter χ^2/dof is calculated as the sum of the squares of the deviations between the measured data and the fit, divided by the total number of data points used, minus two.

Data sets	$\alpha_d^{(a)}$	$\alpha_q^{(a)}$	χ^2/dof
Berl	9.059(18)	19.1(1.4)	0.05
Berl, Lee	9.096(21)	16.3(1.7)	2.9
Berl, Lee, Moore	9.089(6)	16.8(6)	2.7

involve g -state measurements, except for the Lee results at low $\Delta_q^{(a)}/\Delta_d^{(a)}$ which are relatively imprecise. A possible explanation is that the stray fields in our experiment are larger than estimated, which would tend to decrease the measured $h - i$ intervals as seen. Alternatively, the core-penetration effect in the g states may be larger than expected. This would tend to increase the measured values for those states, which is also consistent. Our error analysis accounts for this tension by increasing the fit uncertainty in the parameters as explained above.

However, the adiabatic approximation is inadequate here and must be corrected to incorporate non-adiabatic effects [21, 22, 29–31]. The non-adiabatic correction arises because Eq. (2) is an approximation to the second-order shift from the multipole expansion of the Coulomb interaction between the Rb^+ ion core and the Rydberg electron. The same method of analyzing the experimental data can be used if we introduce correction factors $k_{d,n\ell}$ and $k_{q,n\ell}$ into Eq. (1), which then reads [19, 32]

$$W = -\frac{1}{2}k_{d,n\ell}\alpha_d \left\langle \frac{1}{r^4} \right\rangle_{n\ell} - \frac{1}{2}k_{q,n\ell}\alpha_q \left\langle \frac{1}{r^6} \right\rangle_{n\ell}. \quad (6)$$

To develop an estimation for k_d and k_q , we consider the contribution of the dipole polarizability to the polarization shift of a $\text{Rb } n\ell$ state [22, 32]. The atomic wavefunction is taken to be a direct product of the ion wavefunction and a hydrogenic wavefunction for the Rydberg electron. Consequently, the total energy is simply the sum of the ion and Rydberg energies. In a bound $\text{Rb } n\ell$ state, the Rydberg electron is coupled to the ground $4p^6$ state of Rb^+ , which we denote as a , so the bound Ryd-

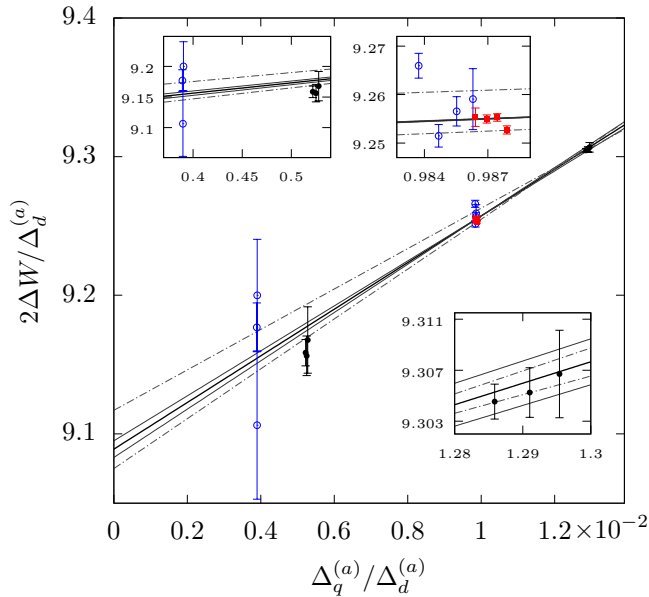


FIG. 5. (color online) Core polarizability analysis in the adiabatic approximation. Solid black circles correspond to measurements reported here, open blue circles are values from Lee *et al.* [12], and solid red squares are from Moore *et al.* The axis quantities are discussed in the text, and given in atomic units (a_0^3 for the vertical axis, and a_0^{-2} for the horizontal axis). The heavy solid line is a linear fit to all the data shown, weighted by the individual error bars. The thin solid lines show the effect of varying the slope and intercept across their 1σ -confidence interval. The dashed lines show the confidence interval obtained using only the Berl and Lee data. The intercept and slope of the line give, respectively, the dipole and quadrupole polarizabilities in the adiabatic approximation. Insets show expanded views near each set of points.

berg state is denoted $an\ell$. Similarly, a Rydberg $n'\ell'$ electron coupled to an excited state b of Rb^+ is denoted $bn'\ell'$. We restrict our attention to ion states which are dipole coupled to the ground state. In the Rydberg atom, the $an\ell$ state is coupled by the dipole term of the Coulomb expansion to the $bn'(\ell-1)$ and $bn'(\ell+1)$ states, as well as the $be'(\ell-1)$ and $be'(\ell+1)$ continua. The resulting second-order dipole energy shift of the $an\ell$ state is given explicitly by [19, 22]

$$\Delta W_{d,n\ell} = \frac{1}{3} \sum_{b,n'} \left[\frac{\ell \langle a|r_1|b \rangle^2 \langle n\ell|r_2^{-2}|n'(\ell-1) \rangle^2}{(2\ell+1)(W_{an\ell} - W_{bn'(\ell-1)})} + \frac{(\ell+1) \langle a|r_1|b \rangle^2 \langle n\ell|r_2^{-2}|n'(\ell+1) \rangle^2}{(2\ell+1)(W_{an\ell} - W_{bn'(\ell+1)})} \right], \quad (7)$$

where the sums are understood to include the continua above the Rydberg and ion limits. Here r_1 represents a core electron and r_2 the Rydberg electron. The r_2^{-2} matrix elements are computed using Numerov's method,

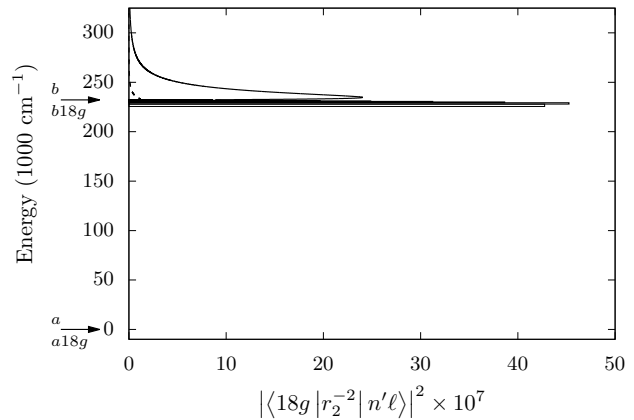


FIG. 6. Energy distribution of the $18g$ Rydberg matrix elements. The vertical axis is the energy of the Rydberg atom, with the core ion ground state a and excited state b indicated by arrows. The energy difference between the ion states and the Rydberg atom states $a18g$ and $b18g$ is too small to resolve. The horizontal axis shows the square matrix elements to the $bn'f$ and $bn'h$ states, and also to the $be'f$ and $be'h$ continua. The continuum states are normalized per unit energy and the bound states are plotted as boxes normalized per unit energy. Values for the h states are shown with dashed lines, but the f state matrix elements are generally much larger. The energy range over which the matrix elements remain appreciable is seen to be small, but not very small, compared to $W_b - W_a$. Here we take $W_b = 232\,300\text{ cm}^{-1}$, corresponding to the effective ion excitation energy W_{Id} discussed in the text.

and their accuracy is verified using the sum rule [22]

$$\langle n\ell|r^{2s}|n\ell \rangle = \sum_{n'} \langle n\ell|r^s|n'\ell' \rangle^2. \quad (8)$$

The energy denominators of Eq. (7) can be rewritten as

$$W_{an\ell} - W_{bn'\ell'} = W_a - W_b + W_{n\ell} - W_{n'\ell'} \quad (9)$$

The adiabatic expression of Eq. (2) is the result of taking $W_{n\ell} - W_{n'\ell'} = 0$, since it is much smaller than $W_b - W_a$. However, the squared $\langle n\ell|r_2^{-2}|n'\ell' \rangle$ matrix elements cover a substantial energy range, as shown by the $18g$ example in Fig. 6. Here the matrix elements cover an energy range that is about 15% of $W_b - W_a$. The energy range does not depend strongly on the Rydberg state energy, so we expect the k_d coefficients in Eq. (6) to largely independent of n .

Rather than neglecting $W_{n\ell} - W_{n'\ell'}$ entirely, we consider Taylor expanding Eq. (7) with $|W_{n\ell} - W_{n'\ell'}|/|W_a - W_b|$ as a small parameter. To first order, it is possible to show that the sum over the ionic core transitions can be replaced by an effective transition to a single ion state at

energy W_{Id} above the ground state, with W_{Id} given by

$$\frac{1}{W_{Id}} = \frac{\sum_b \frac{\langle a|r_1|b\rangle^2}{(W_a - W_b)^2}}{\sum_b \frac{\langle a|r_1|b\rangle^2}{W_a - W_b}}, \quad (10)$$

which is an appropriately weighted average of $1/(W_a - W_b)$. Similarly, we can obtain an effective matrix element

$$\langle a|r_1|I\rangle^2 = \frac{\left(\sum_b \frac{\langle a|r_1|b\rangle^2}{W_a - W_b}\right)^2}{\sum_b \frac{\langle a|r_1|b\rangle^2}{(W_a - W_b)^2}}. \quad (11)$$

Replacing the sum over the excited states of the ion with the effective state I allows the ion dipole matrix element to be removed from the sum, leaving

$$\Delta W_{d,n\ell} = \frac{1}{3} \langle a|r_1|I\rangle^2 \sum_{n'} \left[\frac{\ell \langle n\ell|r_2^{-2}|n'(\ell-1)\rangle^2}{(2\ell+1)(W_{an\ell} - W_{In'(\ell-1)})} + \frac{(\ell+1) \langle n\ell|r_2^{-2}|n'(\ell+1)\rangle^2}{(2\ell+1)(W_{an\ell} - W_{In'(\ell+1)})} \right], \quad (12)$$

In practice, it is not necessary to evaluate $\langle a|r_1|I\rangle^2$ since in this approximation, the ion polarizability is itself simply $\langle a|r_1|I\rangle^2/6W_{Id}$.

We do need to determine W_{Id} , which requires a knowledge of the distribution of oscillator strength f_a from the ion ground state. Unfortunately, this is not well known. However, the photoionization cross section, proportional to df_a/dW , is known and similar to the photoionization cross section of the isoelectronic neutral Kr [33, 34]. For Kr the oscillator strengths are known for both the bound states and the continuum [35], and using them we computed W_{Id} for Kr. We find a value 6% higher in energy than the first ionization limit of Kr at 112 900 cm^{-1} . We estimate the value for Rb^+ to also be 6% higher than the ionization limit at 220 100 cm^{-1} , resulting in $W_{Id} = 232\,300 \text{ cm}^{-1}$.

Using $\langle a|r_1|I\rangle^2/3 = 2\alpha_d W_{Id}$, we can obtain an expression for k_d as

$$k_{d,n\ell} = \frac{W_{Id}}{\langle n\ell|r_2^{-4}|n\ell\rangle} \sum_{n'} \left[\frac{\ell \langle n\ell|r_2^{-2}|n'(\ell-1)\rangle^2}{(2\ell+1)(W_{an\ell} - W_{In'(\ell-1)})} + \frac{(\ell+1) \langle n\ell|r_2^{-2}|n'(\ell+1)\rangle^2}{(2\ell+1)(W_{an\ell} - W_{In'(\ell+1)})} \right]. \quad (13)$$

The values of k_d computed in this way are given in Table III.

To obtain an estimate of the uncertainty in k_d , we note that W_{Id} is roughly bounded by the lowest ionic excited state energy and the second ionization energy. For instance, a calculation of W_{Id} in atomic hydrogen gives a

TABLE III. Non-adiabatic correction factors, calculated as in Eq. (13). The lower- n values are relevant to the data taken here, and the higher- n values are for the data of Ref. [12].

n	k_d			k_q		
	$\ell=4$	5	6	4	5	6
17-19	0.978(2)	0.990(1)	0.994(1)	0.919(15)	0.966(7)	0.984(3)
27-42	0.977(2)	0.990(1)		0.919(15)	0.966(7)	

value just above the $1s - 2p$ transition energy, which reflects the fact that this transition contains over half of the total oscillator strength. In contrast, neutral Kr has six times as much oscillator strength in the first 20 eV above the ionization limit as in the bound states [35], which explains why W_{Id} is comparable to the ionization energy in that case. The first excited state of Rb^+ lies at 134 000 cm^{-1} , about 40% below the ionization limit. This sets the scale for the uncertainty range, but we believe the isoelectronic analogy to Kr to be reasonably sound, so we estimate an uncertainty of $\pm 10\%$ for W_{Id} . This translates directly to a 10% uncertainty in $(1 - k_{d,n\ell})$ and provides the uncertainties shown in Table III.

The quadrupole correction factor $k_{q,n\ell}$ is calculated in much the same way as $k_{d,n\ell}$. In this case the $\langle n\ell|r_2^{-3}|n'\ell'\rangle$ matrix elements are required, and they are similarly evaluated numerically for hydrogenic wave functions. To assign an effective energy W_{Iq} accounting for the ionic quadrupole transitions, we use an expression analogous to Eq. (10). Lacking better information, we calculate W_{Iq} for hydrogen and obtain 122 465 cm^{-1} , which is 12% over the ionization limit. The ground state of Rb^{++} is split by the spin-orbit interaction, so we use the center of gravity of the spin-orbit split state as the Rb^+ limit. Assuming W_{Iq} to lie 12% above this results in $W_{Iq} = 248\,000 \text{ cm}^{-1}$. Using this value of W_{Iq} in the quadrupole analog of Eq. (13), we calculate $k_{q,n\ell}$. Since there is no analog to the Kr oscillator strength distribution for comparison, we assign a $\pm 20\%$ uncertainty to W_{Iq} and thus to $1 - k_{q,n\ell}$. The results are also shown in Table III.

Since we measure energy differences ΔW , we again use Eq. (3), but the definitions of Δ_d and Δ_q now include $k_{d,n\ell}$ and $k_{q,n\ell'}$ and are given by

$$\Delta_d \equiv k_{d,n\ell} \left\langle \frac{1}{r^4} \right\rangle_{n\ell} - k_{d,n\ell'} \left\langle \frac{1}{r^4} \right\rangle_{n\ell'} \quad (14)$$

and

$$\Delta_q \equiv k_{q,n\ell} \left\langle \frac{1}{r^6} \right\rangle_{n\ell} - k_{q,n\ell'} \left\langle \frac{1}{r^6} \right\rangle_{n\ell'}. \quad (15)$$

As before, we plot $2\Delta W/\Delta_d$ vs. Δ_q/Δ_d , for (ℓ, ℓ') pairs (4, 5) and (5, 6), shown as the solid circles in Fig. 7. Open circles are again data from Lee *et al.* [12], and closed squares are from Moore *et al.* [18], with the Lee data plotted as $2W/(k_d \langle r^{-4} \rangle)$ vs. $(k_q \langle r^{-6} \rangle)/(k_d \langle r^{-4} \rangle)$. The heavy

TABLE IV. Calculated values of the dipole and quadrupole polarizabilities, incorporating non-adiabatic corrections. Data sets are the same as in Table II. Here the first value in parentheses is the estimated error from the linear fit, and the second value is the estimated error from the non-adiabatic corrections. The bottom row shows our final estimated values with uncertainties, taken from the fit with all three data sets.

Data sets	$\alpha_d^{(a)}$	$\alpha_q^{(a)}$	χ^2/dof
Berl	9.060(19)(10)	42.9(1.6)(6.3)	0.11
Berl, Lee	9.120(29)(7)	38.1(2.6)(5.6)	4.4
Berl, Lee, Moore	9.116(6)(7)	38.4(0.7)(5.6)	3.7
Final values	9.116(9)	38.4(6)	

line is a fit to all the data, while the thin and dashed lines show the confidence intervals with and without the Moore data, respectively. The fit results are listed in Table IV, with the first values in parentheses indicating the estimated uncertainties.

These fits do not account for the uncertainties in k_d and k_q themselves. To do so, we redo the analysis as the W_I and W_{Iq} parameters are varied independently across their uncertainty ranges. The resulting changes in polarizabilities are indicated in Table IV by the second value in parentheses. We take the total uncertainty as the quadrature sum of the two values, leading to final results of $\alpha_d = 9.12(3)$, $\alpha_q = 38.1(6)$ for the Berl and Lee data only, and $\alpha_d = 9.116(9)$, $\alpha_q = 38.4(6)$ when the Moore data is included. The value of α_d is only 0.3% different from its adiabatic value, almost in agreement with the adiabatic expansion model, which predicts no change [36, 37]. However, α_q is almost double its adiabatic value, due primarily to k_q .

Our results can be compared to previous theoretical estimates summarized in Table V. We find good agreement with the most recent results of [3]. This consistency resolves the large discrepancy between theory and the adiabatic α_q value reported in [12].

Although we measure transition frequencies, we can use the extracted polarizabilities to calculate the absolute energy of the Rydberg states, and thus obtain the quantum defects. For this, we use Eq. (2) and the adiabatic polarizability values $\alpha_d^{(a)}$ and $\alpha_q^{(a)}$, since that avoids the uncertainty in the non-adiabatic correction factors. The

TABLE V. Theoretical estimates of the core polarizability parameters.

Ref.	α_d (au)	α_q (au)
[3]	9.1	35.4
[38]	9.076	35.41
[23]	10.22	
[24]		38.43

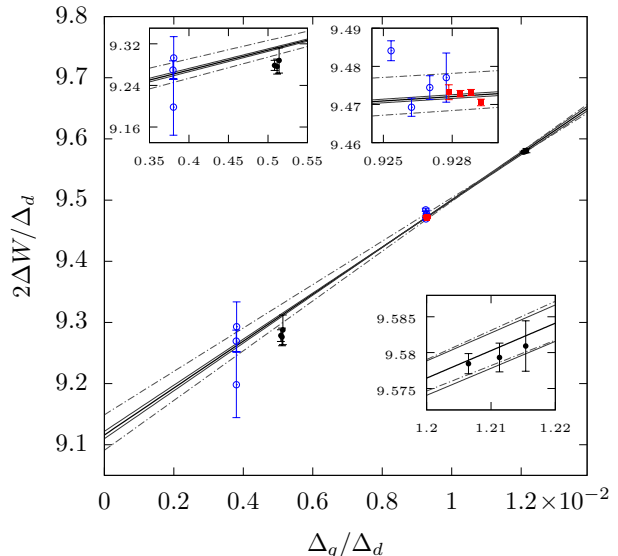


FIG. 7. (color online) Core polarizability analysis including non-adiabatic corrections. As in Fig. 5, solid black circles are measurements from the present work, open blue points are from Lee *et al.* [12], and solid red squares are from Moore *et al.* [18]. The axis quantities now include the non-adiabatic correction factors k_d and k_q , as discussed in the text. Quantities are in atomic units, a_0^3 (vertical) and a_0^{-2} (horizontal). The heavy solid line is a fit to all the data. The thin solid lines illustrate the uncertainty in the fit, and the dashed lines show the confidence range using only the Berl and Lee data. The uncertainties here do not include the uncertainties of the non-adiabatic coefficients k_i .

quantum defects are then found by setting

$$W_{n\ell} = \frac{R}{n^2} - \frac{R}{(n - \delta_{n\ell})^2}. \quad (16)$$

We use the Ritz expansion [39]

$$\delta(n) = \delta_0 + \frac{\delta_2}{(n - \delta_0)^2}. \quad (17)$$

By expanding both Eq. (2) and Eq. (17) in powers of $1/n$ and matching coefficients, we have

$$\delta_{0,\ell} = \frac{1}{R} \left[\frac{12(2\ell - 2)!}{(2\ell + 3)!} \alpha_d^{(a)} + \frac{560(2\ell - 4)!}{(2\ell + 5)!} \alpha_q^{(a)} \right] \quad (18)$$

and

$$\delta_{2,\ell} = -2\delta_0^3 - \frac{1}{R} \left\{ \frac{4\ell(\ell + 1)(2\ell - 2)!}{(2\ell + 3)!} \alpha_d^{(a)} + \frac{480(2\ell - 4)!}{(2\ell + 5)!} \left[\ell(\ell + 1) - \frac{5}{6} \right] \alpha_q^{(a)} \right\}. \quad (19)$$

We use these expressions and the $\alpha_i^{(a)}$ values calculated with the Moore data to find the results listed in Table VI. The g -state values can be compared to $\delta_0 =$

TABLE VI. Quantum defect Ritz expansion coefficients of Eq. (17).

ℓ	δ_0	δ_2
g	0.004 007(5)	-0.027 42(6)
h	0.001 423(1)	-0.014 38(2)
i	0.000 607 4(4)	-0.008 550(8)

0.00400(2), $\delta_2 = -0.018(15)$ obtained by Lee [12] and $\delta_0 = 0.003999(2)$, $\delta_2 = -0.020(2)$ obtained by Moore [18]. The source of this discrepancy is likely related to the moderate inconsistencies of the measurements noted in Table II. We expect these inconsistencies to be resolved with further investigations.

IV. CONCLUSIONS

The measurements reported here provide a new set of constraints on the core polarizabilities of Rb atoms, based on relatively low n values. Together with new high- n results from Moore *et al.* [18], the precisions of α_d and α_q are improved by a factor of four compared to the previous work of Lee *et al.* [12]. In addition, we point out that non-adiabatic effects have a significant impact on the value of the quadrupole polarizability α_q , which brings the experimental results into line with theory.

We can consider methods to further improve the measurements. Since uncertainty in the non-adiabatic corrections is significant, it would be helpful to determine them with a more sophisticated atomic structure calculation, compared to the empirical approach described here. If such a calculation can be performed, then reducing the measurement uncertainties would also be useful. A straightforward improvement would be to add electrodes to the apparatus to allow control of the transverse electric field, so that dc Stark shifts can be further reduced.

Extending the measurements to even higher ℓ would provide a useful test of the core polarization model, and help identify any penetration shifts in the g -states. However, this is challenging because the signal-to-noise ratio on the $nf \rightarrow nj$ transition would be low in our existing apparatus. Further, the decreasing value of ΔW makes the relative frequency uncertainty more significant. A different approach would be to perform absolute spectroscopy of the nf state so that the energy shifts relative to hydrogen of the ng , nh and ni states could be used independently. We cannot carry out such spectroscopy with our current apparatus: although precise spectroscopy of the nd states is available [40], at low n values the $nd - nf$ frequency intervals are too large to access with our microwave technology.

We expect that the improved core polarizability values determined in this work will be useful for precision measurements such as atomic clocks and tune-out spectroscopy. In regards to our own interest in tune-out spectroscopy, the core polarizability was a source of uncertainty in the determination of the ratio of the $5p_{3/2}$ to $5p_{1/2}$ dipole matrix elements. The original analysis in [10] used $\alpha_d = 9.08(10)$ au. Using the value 9.116(9) determined here, we find that the ratio is slightly reduced, from 1.99 217(3) to 1.992 15(3). We hope that further improvements will allow us to reduce the uncertainty in this value and to better constrain other dipole matrix elements of Rb as well [10].

ACKNOWLEDGMENTS

This work was supported by National Science Foundation (grant Number PHY-1607571) and the Air Force Office of Scientific Research (grant Number FA9550-14-1-0288). J. Nunkaew was supported by the Thailand Center of Excellence in Physics (ThEP-61-PHY-MU3). It is a pleasure to acknowledge Adam Fallon and Safra Niyaz for useful discussions.

-
- [1] L. J. LeBlanc and J. H. Thywissen, Species-specific optical lattices, *Phys. Rev. A* **75**, 053612 (2007).
 - [2] J. Mitroy, M. S. Safronova, and C. W. Clark, Theory and applications of atomic and ionic polarizabilities, *J. Phys. B: At. Mol. Opt. Phys.* **43**, 202001 (2010).
 - [3] M. S. Safronova and U. I. Safronova, Critically evaluated theoretical energies, lifetimes, hyperfine constants, and multipole polarizabilities in ^{87}Rb , *Phys. Rev. A* **83**, 052508 (2011).
 - [4] V. A. Dzuba, V. V. Flambaum, and B. Roberts, Calculation of the parity-violating $5s-6s$ $E1$ amplitude in the rubidium atom, *Phys. Rev. A* **86**, 062512 (2012).
 - [5] C. Gaiser and B. Fellmuth, Polarizability of helium, neon, and argon: New perspectives for gas metrology, *Phys. Rev. Lett.* **120**, 123203 (2018).
 - [6] C. R. Ekstrom, J. Schmiedmayer, M. S. Chapman, T. D. Hammond, and D. E. Pritchard, Measurement of the electric polarizability of sodium with an atom interferometer, *Phys. Rev. A* **51**, 3883 (1995).
 - [7] A. Miffre, M. Jacquy, M. Büchner, G. Tréneç, and J. Vigué, Measurement of the electric polarizability of lithium by atom interferometry, *Phys. Rev. A* **73**, 011603 (2006).
 - [8] W. F. Holmgren, M. C. Reville, V. P. A. Lonij, and A. D. Cronin, Absolute and ratio measurements of the polarizability of Na, K, and Rb with an atom interferometer, *Phys. Rev. A* **81**, 053607 (2010).
 - [9] M. D. Gregoire, I. Hromada, W. F. Holmgren, R. Trubko, and A. D. Cronin, Measurements of the ground-state polarizabilities of Cs, Rb, and K using atom interferometry, *Phys. Rev. A* **92**, 052513 (2015).
 - [10] R. H. Leonard, A. J. Fallon, C. A. Sackett, and M. S.

- Safronova, High-precision measurements of the ^{87}Rb D-line tune-out wavelength, *Phys. Rev. A* **92**, 052501 (2015).
- [11] A. Fallon and C. Sackett, Obtaining atomic matrix elements from vector tune-out wavelengths using atom interferometry, *Atoms* **4**, 12 (2016).
- [12] J. Lee, J. Nunkaew, and T. F. Gallagher, Microwave spectroscopy of the cold rubidium $(n+1)d_{5/2} \rightarrow ng$ and nh transitions, *Phys. Rev. A* **94**, 022505 (2016).
- [13] R. Trubko, M. D. Gregoire, W. F. Holmgren, and A. D. Cronin, Potassium tune-out-wavelength measurement using atom interferometry and a multipass optical cavity, *Phys. Rev. A* **95**, 052507 (2017).
- [14] B. Arora, M. S. Safronova, and C. W. Clark, Tune-out wavelengths of alkali-metal atoms and their applications, *Phys. Rev. A* **84**, 043401 (2011).
- [15] M. D. Gregoire, N. Brooks, R. Trubko, and A. Cronin, Analysis of polarizability measurements made with atom interferometry, *Atoms* **4** (2016).
- [16] M. Born and W. Heisenberg, Über den Einfluß der Deformierbarkeit der Ionen auf optische und chemische Konstanten. I, *Zeitschrift für Physik* **23**, 388 (1924).
- [17] B. Edlén, *Handuch der Physik*, edited by S. Flügge (Springer, Berlin, 1964) pp. 80–220.
- [18] K. Moore, A. Duspayev, R. Cardman, and G. Raithel, Measurement of rb g-series quantum defect using two-photon microwave spectroscopy (2020), [arXiv:2004.11407 \[physics.atm-clus\]](https://arxiv.org/abs/2004.11407).
- [19] T. F. Gallagher, *Rydberg Atoms* (Cambridge University, 1994) p. 348.
- [20] N. G. Whitelaw and J. H. Van Vleck, *Phys. Rev.* **41**, 389A (1932).
- [21] J. E. Mayer and M. G. Mayer, The polarizabilities of ions from spectra, *Phys. Rev.* **43**, 605 (1933).
- [22] J. H. Van Vleck and N. G. Whitelaw, The quantum defect of nonpenetrating orbits, with special application to Al II, *Phys. Rev.* **44**, 551 (1933).
- [23] J. Heinrichs, Simple Calculation of Polarizabilities, Hyperpolarizabilities, and Magnetic Susceptibilities of Atoms and Ions, *The Journal of Chemical Physics* **52**, 6316 (1970).
- [24] R. M. Sternheimer, Quadrupole Polarizabilities of Various Ions and the Alkali Atoms, *Physical Review A* **1**, 321 (1970).
- [25] M. L. Zimmerman, M. G. Littman, M. M. Kash, and D. Kleppner, Stark structure of the rydberg states of alkali-metal atoms, *Phys. Rev. A* **20**, 2251 (1979).
- [26] J. Han, Y. Jamil, D. V. L. Norum, P. J. Tanner, and T. F. Gallagher, Rb nf quantum defects from millimeter-wave spectroscopy of cold ^{85}Rb Rydberg atoms, *Phys. Rev. A* **74**, 054502 (2006).
- [27] N. H. Tran, H. B. van Linden van den Heuvell, R. Kachru, and T. F. Gallagher, Radiofrequency resonance measurements of Na $d-f$ intervals, *Phys. Rev. A* **30**, 2097 (1984).
- [28] H. A. Bethe and E. E. Salpeter, *Quantum mechanics of one and two electron atoms* (Springer, 1957) p. 17.
- [29] R. R. Freeman and D. Kleppner, Core polarization and quantum defects in high-angular-momentum states of alkali atoms, *Phys. Rev. A* **14**, 1614 (1976).
- [30] H. Eissa and U. pik, The polarization of a closed-shell core of an atomic system by an outer electron I. a correction to the adiabatic approximation, *Proceedings of the Physical Society* **92**, 556 (1967).
- [31] M. Peper, F. Helmrich, J. Butscher, J. A. Agner, H. Schmutz, F. Merkt, and J. Deiglmayr, Precision measurement of the ionization energy and quantum defects of ^{39}K i, *Phys. Rev. A* **100**, 012501 (2019).
- [32] T. F. Gallagher, R. Kachru, and N. H. Tran, Radio frequency resonance measurements of the Ba $6sng-6snh-6sni-6snk$ intervals: An investigation of the nonadiabatic effects in core polarization, *Phys. Rev. A* **26**, 2611 (1982).
- [33] B. M. McLaughlin and J. F. Babb, Single photoionization of the Kr-like Rb II ion in the photon energy range 2246.0eV, *Monthly Notices of the Royal Astronomical Society* **486**, 245 (2019).
- [34] J. A. Samson, The measurement of the photoionization cross sections of the atomic gases (Academic Press, 1966) pp. 177 – 261.
- [35] J. Berkowitz, Chapter V - Total photoabsorption and photoionization cross sections for selected molecules, in *Photoabsorption, Photoionization, and Photoelectron Spectroscopy*, edited by J. Berkowitz (Academic Press, 1979) pp. 73 – 154.
- [36] C. J. Kleinman, Y. Hahn, and L. Spruch, Dominant nonadiabatic contributions to the long range electron-atom interaction, *Phys. Rev.* **165**, 53 (1968).
- [37] E. L. Snow and S. R. Lundeen, Higher order contributions to the fine structure in high- l rydberg states of si^{2+} , *Phys. Rev. A* **75**, 062512 (2007).
- [38] W. Johnson, D. Kolb, and K.-N. Huang, Electric-dipole, quadrupole, and magnetic-dipole susceptibilities and shielding factors for closed-shell ions of the He, Ne, Ar, Ni (Cu+), Kr, Pb, and Xe isoelectronic sequences, *Atomic Data and Nuclear Data Tables* **28**, 333 (1983).
- [39] G. W. F. Drake and R. A. Swainson, Expectation values of r^p for arbitrary hydrogenic states, *Phys. Rev. A* **42**, 1123 (1990).
- [40] W. Li, I. Mourachko, M. W. Noel, and T. F. Gallagher, Millimeter-wave spectroscopy of cold Rb Rydberg atoms in a magneto-optical trap: Quantum defects of the ns, np, and nd series, *Phys. Rev. A* **67**, 052502 (2003).